![The University of Edinburgh logo]

THE UNIVERSITY of EDINBURGH

Edinburgh Research Explorer

Lattice determination of the hadronic contribution to the muon g-2 using dynamical domain wall fermions

OPEN ACCESS

Lattice determination of the hadronic contribution to the muon $g - 2$ using dynamical domain wall fermions

Peter Boyle, Luigi Del Debbio, Eoin Kerrane, and James Zanotti

We present a calculation of the leading-order hadronic contribution to the anomalous magnetic moment of the muon for a dynamical simulation of $2 + 1$ flavor QCD using domain wall fermions. The electromagnetic 2-point function is evaluated on the lattice gauge configurations and this is fitted to a continuous form motivated by models of vector dominance. We find broad agreement with previous lattice results for this quantity, while improvements in simulation and theory are clearly needed in order to produce satisfactorily precise results.

I. INTRODUCTION

The anomalous magnetic moment a of a lepton is half the discrepancy from 2 ($a = \frac{g-2}{2}$) of g, the gyromagnetic ratio or Landé g factor, which relates the spin $\vec{S}$ of the lepton to its magnetic moment $\vec{\mu}$ as

$$\vec{\mu} = g\frac{e}{2m}\vec{S}. \tag{1.1}$$

It is given the name "anomalous" because it is a purely quantum effect and so is zero in a classical theory.

The one-loop computation of the electron anomalous magnetic moment a_e by Schwinger [1] was one of the first such calculations, and provided strong evidence in support of the young theory of QED by explaining observed hyperfine phenomena which were not well understood. Since then, a_e has become possibly the most accurately determined quantity in science, being known to a precision better than one part per billion [2]. The corresponding theoretical calculation has achieved similar accuracy [3]. Because of the relatively light mass of the electron, the calculation is strongly dominated by QED contributions with virtual electrons, which are known to a good accuracy to four-loops. Using an independent determination of the fine-structure constant α from atomic interferometry results in a value of a_e which agrees with the experimental result, with an uncertainty over 30 times greater. Combining the experimental and theoretical results for a_e in terms of the fine-structure constant α provides the most accurate available determination of α [2].

Because of its heavier mass, $\frac{m_\mu^2}{m_e^2} \simeq 400\,00$, the muon anomalous magnetic moment a_μ is far more sensitive to contributions from other sectors of the standard model, as well as to any potential new-physics contributions. This makes it a far more robust test of the standard model, and a much more interesting searching ground for signals of new physics. The current experimental result, while not nearly as accurate as that for a_e, is still remarkably precise [4]:

$$a_\mu = 11\,659\,208.0(6.3) \times 10^{-10}, \tag{1.2}$$

which remains a precision of better than one part per million.

Obtaining a theoretical result for a_μ of comparable precision has proved a more difficult task than in the case of a_e [5]. This is because, as stated above, the contributions from other sectors of the standard model are more significant. However, the calculation has been brought to a point where the uncertainty is of the same order as the experimental uncertainty. Interestingly however, there is a discrepancy between the two values which exceeds the current uncertainty. This has attracted a huge amount of interest to a_μ and lead to significant efforts to calculate contributions from potential new-physics sectors.

The current uncertainty in a_μ is strongly dominated by hadronic contributions, specifically the leading-order hadronic, and hadronic light-by-light contributions. The light-by-light contribution has attracted significant theoretical interest, and has recently become the focus of considerable work using lattice simulations [6,7].

This work involves the leading-order hadronic contribution, which we denote as $a_\mu^{(2)\text{had}}$, the best estimate of which is currently obtained by relating the hadronic vacuum polarization of the photon to the cross section for e^+e^- decay into hadrons, allowing a dispersive integral over experimental data for the cross section [8].

Despite the apparent accuracy of the results obtained from this procedure, there remain discrepancies between results from different data sets. As a result, it is not clear if this method of obtaining the vacuum polarization is under good control [5,8]. Attempts have also been made to estimate this quantity using models of low-energy QCD [9]. It would, however, be preferable to obtain the hadronic contribution to a_μ from a first principles approach. For this, the only valid candidate is lattice QCD which alone is capable of producing quantitative results from fully nonperturbative QCD.
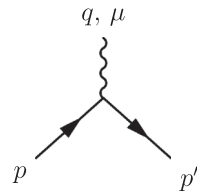
This quantity was first tackled through lattice computation in quenched simulations first with domain wall fermions [10], followed by a calculation with improved Wilson fermions [11]. The first dynamical simulation followed

[12,13] using $2 + 1$ flavor staggered quarks, and several studies of this quantity are ongoing, using 2 flavors of improved Wilson fermions [14] and twisted mass fermions [15]. We present a calculation of $a_\mu^{(2)\text{had}}$ from a dynamical simulation of $2 + 1$ flavor QCD with domain wall fermions.
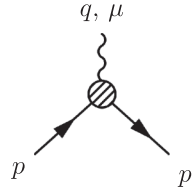
II. BACKGROUND

The Landé g factor of a fermion can be expressed in terms of the electromagnetic form factors F_1 and F_2 as

$$g = 2[F_1(0) + F_2(0)]. \quad (2.1)$$

$$= -ie\Gamma_\mu(p', p) \equiv -ie\left[\gamma_\mu F_1(q^2) + \frac{i\sigma^{\mu\nu}q_\nu}{2m}F_2(q^2)\right]. \quad (2.3)$$

From the Born approximation, it can be seen that $F_1(0) = 1$ to all orders, and so

$$a = \frac{g - 2}{2} = F_2(0). \quad (2.4)$$

We seek to compute the effect of hadronic vacuum polarization contributions to a_μ which are obtained by calculating contributions to the graph in (2.3) of the form

These form factors are defined in the effective electromagnetic scattering vertex whereby the expression for the tree-level graph

$$= -ie\gamma_\mu \quad (2.2)$$

is replaced by its equivalent including all quantum corrections

As described in [10], the contribution to a_μ from the one-loop diagram equivalent to the graph (2.5) with the hadronic blob removed can be expressed as

$$\longrightarrow a_\mu^{(1)} = \frac{\alpha}{\pi}\int_0^\infty dQ^2 \, f(Q^2) \quad (2.6)$$

where the kernel function $f(Q^2)$ is divergent as $Q^2 \to 0$ and can be expressed

$$f(Q^2) = \frac{m_\mu^2 Q^2 Z(Q^2)^3 (1 - Q^2 Z(Q^2))}{1 + m_\mu^2 Q^2 Z(Q^2)^2},$$

$$Z(Q^2) = -\frac{Q^2 - \sqrt{Q^4 + 4m_\mu^2 Q^2}}{2m_\mu^2 Q^2}. \quad (2.7)$$

From this, the expression for the hadronic vacuum polarization contribution can be obtained with the insertions:

$$\longrightarrow a_\mu^{(2)had} = \left(\frac{\alpha}{\pi}\right)^2 \int_0^\infty dQ^2 \, f(Q^2) \times \hat{\Pi}(Q^2) \quad (2.8)$$

where $\hat{\Pi}(Q^2)$ is the infrared subtracted transverse part of the hadronic vacuum polarization

$$\hat{\Pi}(Q^2) = \Pi(Q^2) - \Pi(0),$$

$$\Pi_{\mu\nu}(q) = (q^2 g_{\mu\nu} - q_\mu q_\nu)\Pi(q^2), \quad (2.9)$$

$$q, \mu \quad \text{had} \quad q, \nu \equiv i\Pi_{\mu\nu}(q) \quad (2.10)$$

at Euclidean momentum $Q^2 = -q^2$. The hadronic vacuum polarization function $\Pi_{\mu\nu}(q)$ can be computed as the Fourier-transformed two-point correlator

$$\Pi_{\mu\nu}(q) = \int d^4x e^{iq\cdot(x-y)}\langle J_\mu(x)J_\nu(y)\rangle \quad (2.11)$$

involving the electromagnetic current

TABLE I. Parameters of the lattice ensembles used in our study.

V	β	a^{-1} GeV	$\hat{q}^2_{\min}$ GeV^2	am_h	am_u
$24^3 \times 64$	2.13	1.73(2)	0.028	0.04	0.02
$24^3 \times 64$	2.13	1.73(2)	0.028	0.04	0.01
$24^3 \times 64$	2.13	1.73(2)	0.028	0.04	0.005
$32^3 \times 64$	2.25	2.28(3)	0.05	0.03	0.008
$32^3 \times 64$	2.25	2.28(3)	0.05	0.03	0.006
$32^3 \times 64$	2.25	2.28(3)	0.05	0.03	0.004
$32^3 \times 64$	1.75	1.375(9)	0.018	0.045	0.0042
$32^3 \times 64$	1.75	1.375(9)	0.018	0.045	0.001

$$J_\mu(x) = \sum_i Q_i \bar{\psi}^i \gamma_\mu \psi^i \qquad (2.12)$$

where ψ^i is the quark field of flavor i and Q^i is its charge. The path integral used in the expectation value in (2.11) will involve only hadronic fields, i.e. quarks and gluons.

A. Simulation

Our computation is performed using configurations generated by the RBC and UKQCD Collaborations as part of their program of investigation using $2 + 1$ flavors of domain wall fermions. We investigate three lattice volumes, each with several ensembles at different values of the light quark mass m_u. The parameters of these ensembles are given in Table I. The ensembles at $\beta = 1.75$ have been generated using a dislocation suppressing determinant ratio (DSDR) in conjunction with the Iwasaki gauge action, with a fifth dimension whose extent is $L_5 = 32$ [16,17]. The lighter of these ensembles is very near to the physical point with a pion mass of $m_\pi \simeq 180$ MeV. The other ensembles used only the Iwasaki action and $L_5 = 16$ [18,19].

The meson masses quoted in Table II might suggest that the vector meson is unstable on a number of these lattices, as its mass is over twice that of the pseudoscalar meson in some cases. However, due to the conservation of angular

TABLE II. Relevant observables measured on our lattices. Results on the $\beta = 1.75$ lattices are preliminary and will be outlined in a forthcoming publication [17], results for f_V on the 64×24^3 lattices are currently unavailable.

β	am_u	Z_V	am_V	am_{PS}	af_V
2.13	0.02	0.696(2)	0.579(6)	0.3227(7)	
2.13	0.01	0.700(2)	0.529(5)	0.2422(5)	
2.13	0.005	0.699(2)	0.505(6)	0.1904(6)	
2.25	0.008	0.7380(5)	0.388(6)	0.1727(4)	0.078(6)
2.25	0.006	0.7385(6)	0.366(5)	0.1512(3)	0.076(5)
2.25	0.004	0.7387(7)	0.356(6)	0.1269(4)	0.070(11)
1.75	0.0042	0.664(5)	0.570(25)	0.1809(3)	0.102(6)
1.75	0.001	0.669(8)	0.558(44)	0.1249(3)	0.105(15)

momentum, the decay cannot occur at zero momentum, and so the energy of the final state is increased. On the lattice, momentum is discrete, and the minimum nonzero momentum that can be assigned to the pseudoscalar mesons forbids the decay of a static vector meson, although on the $\beta = 1.75$ lattices, the truth of this statement is inconclusive given the accuracy of the masses quoted.

B. Vacuum polarization

We compute the lattice vacuum polarization as

$$\tilde{\Pi}_{\mu\nu}(x) = Z_V \sum_i Q_i^2 a^6 \langle \mathcal{V}_\mu^i(x) V_\nu^i(0) \rangle, \qquad (2.13)$$

where we have omitted the flavor-nondiagonal terms as they contain only "disconnected" contributions which are expected to be subdominant, as will be discussed further below.

At the sink, we use the domain wall fermion conserved vector current [20]

$$\mathcal{V}_\mu^i(x) = \sum_{s=1}^{L_5} \frac{1}{2} [\bar{\psi}^i(x + \hat{\mu}, s)(1 + \gamma_\mu) U_\mu^\dagger(x) \psi^i(x, s)$$
$$- \bar{\psi}^i(x, s)(1 - \gamma_\mu) U_\mu(x) \psi^i(x + \hat{\mu}, s)] \qquad (2.14)$$

while at the source we have the local vector current $V_\nu^i(x) = \bar{q}^i(x) \gamma_\nu q^i(x)$ where $q^i(x) = P_+ \psi^i(x, L_5 - 1) + P_- \psi^i(x, 0)$, and $P_\pm = \frac{1}{2}(1 \pm \gamma_5)$. Because of the use of the local vector current, a factor of the vector current renormalization constant, Z_V, is included in our definition of the vacuum polarization. The values of Z_V used on each ensemble are given in Table II, as measured in [19].

These correlators were generated for, and used in, the measurement of the QCD contribution to the electroweak S-parameter [21]. However, they will prove perfectly sufficient for our purposes, as long as we are mindful of Ward identity violations, which will be discussed in Sec. II C.

Of the two Wick contractions arising from this correlator, we compute only the connected one. We leave the evaluation of the disconnected contribution for future work, but note that it is expected to be suppressed relative to the connected contribution [22]. This argument is also the motivation for neglecting the flavor-nondiagonal terms, and we will make an estimate of the systematic uncertainty that results in our conclusions.

We Fourier transform into momentum space:

$$\tilde{\Pi}_{\mu\nu}(\hat{q}) \equiv Z_V \sum_i Q_i^2 \sum_x e^{iqx} a^6 \langle \mathcal{V}_\mu^i(x) V_\nu^i(0) \rangle \qquad (2.15)$$

using the discrete momenta $q_\mu = \frac{2\pi n_\mu}{L_\mu}$ where n_μ is a 4-tuple of integers, and L_μ is the length of the lattice in the μ direction. From here, we will use the lattice momentum

(a) $a\hat{q}_\mu \tilde{\Pi}_{\mu\nu}$ (b) $\tilde{\Pi}_{\mu\nu} a\hat{q}_\nu$
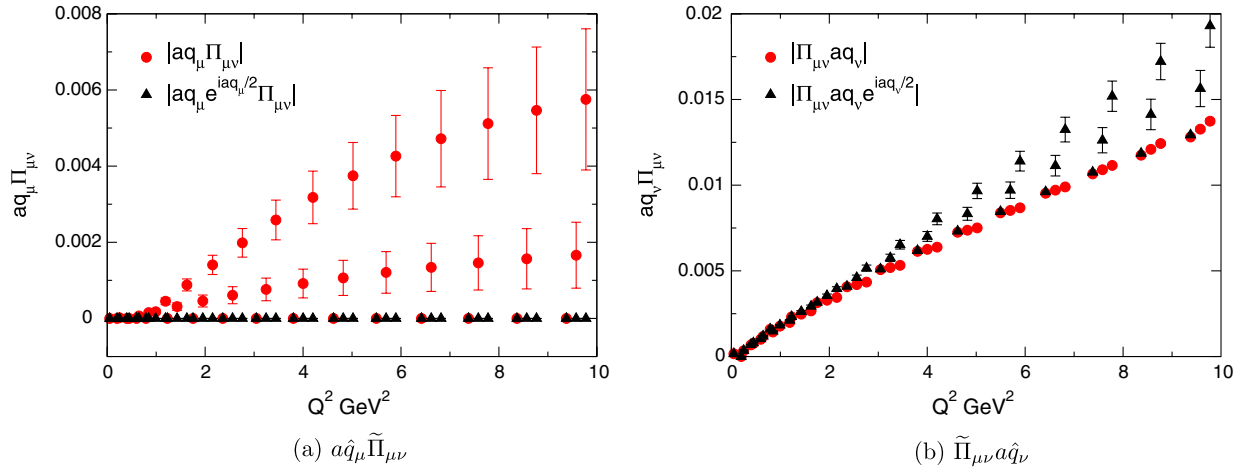
FIG. 1 (color online). Illustration of Ward identity violations in $\Pi_{\mu\nu}$ on $32^3 \times 64$ lattice at $\beta = 2.25$ and $am_u = 0.004$.

$$\hat{q}_\mu = \frac{2}{a} \sin\left(\frac{\pi n_\mu}{L_\mu}\right). \qquad (2.16)$$

We associate the quantity $\hat{q}^2 = \sum_\mu \hat{q}_\mu^2$ with the continuum momentum Q^2.

C. Ward identities

In order to ensure that this reproduces a vacuum polarization of the form (2.9), we must verify that this lattice correlator satisfies the Ward identity $q_\mu \Pi_{\mu\nu} = 0$ which in general is not the case, as although both operators $\mathcal{V}^i$ and V^i have the correct continuum limit

$$\mathcal{V}^i_\mu, V^i_\mu \xrightarrow{a\to 0} J^i = \bar{\psi}^i \gamma_\mu \psi^i \qquad (2.17)$$

the additional irrelevant operators introduced into the lattice action modify the Ward identity for $\tilde{\Pi}_{\mu\nu}$. In coordinate space, the Schwinger-Dyson equation for $\tilde{\Pi}_{\mu\nu}$ reads

$$\langle (\Delta_\mu \mathcal{V}^i_\mu(x)) V^i_\nu(0) \rangle + \left\langle \left(\frac{V^i_\nu(0) \overleftarrow{\partial}}{\partial \psi^i(x)} \psi^i(x) \right) - \left(\bar{\psi}^i(x) \frac{\overrightarrow{\partial} V^i_\nu(0)}{\partial \bar{\psi}^i(x)} \right) \right\rangle$$
$$= 0 \qquad (2.18)$$

where Δ_μ is the backward lattice derivative. Because the local current used is not point-split, the second term in (2.18) vanishes and we have as a result that $e^{(iaq_\mu)/2} \hat{q}_\mu \tilde{\Pi}_{\mu\nu} = 0$.

This is illustrated in Fig. 1 where we see that it is necessary to include the factor $e^{i(aq_\mu)/2}$ in the Ward identity for the first index of $\tilde{\Pi}_{\mu\nu}$, while there is no fulfilled Ward identity for the second index.

D. Decomposing the vacuum polarization

We must extract from $\tilde{\Pi}_{\mu\nu}(\hat{q})$ the scalar vacuum polarization $\tilde{\Pi}(\hat{q}^2)$ which, corresponding to the continuum (2.9), are related by

$$\tilde{\Pi}_{\mu\nu}(\hat{q}) = (\hat{q}^2 \delta_{\mu\nu} - \hat{q}_\mu \hat{q}_\nu) \tilde{\Pi}(\hat{q}^2). \qquad (2.19)$$

In practice, in order to avoid any longitudinal contribution which might arise due to the nonconservation of Ward identities, for each momentum orientation we choose directions μ such that $\hat{q}_\mu = 0$ and compute

$$\tilde{\Pi}(\hat{q}^2) = \frac{\tilde{\Pi}_{\mu\mu}(\hat{q})}{\hat{q}^2} \qquad (2.20)$$

where in the above there is no sum over μ.

In Fig. 2, we show an example of the resulting vacuum polarization function, and compare this to the three-loop continuum perturbation theory result from [23], using two massless flavors of quarks and one massive flavor which we associate with the strange quark. This result is quoted in the $\overline{\text{MS}}$ scheme and as such we require the strange quark mass in our simulations expressed in $\overline{\text{MS}}$. For this, we use the nonperturbative renormalization factor $Z_{mh}^{\overline{\text{MS}}} = 0.1533(6)(33)$ determined in [19]. The factor is quoted in
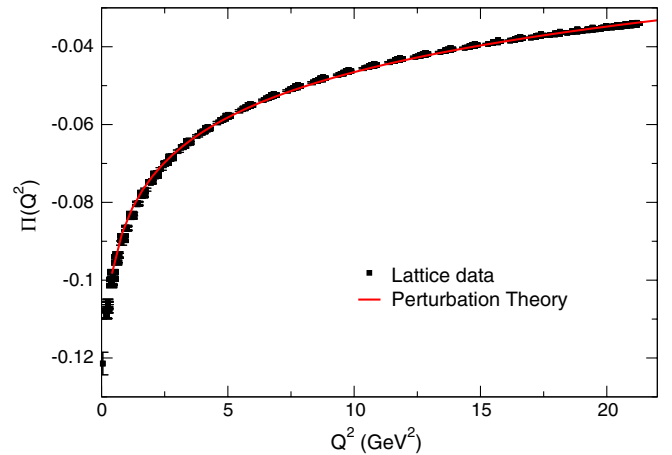

FIG. 2 (color online). Vacuum polarization function $\Pi(Q^2)$ as measured on 64×32^3 lattice at $\beta = 2.25$ and $am_u = 0.004$.

the limit of vanishing light quark mass, but it is also illustrated that the mass dependence is extremely slight, and so we see this as satisfactory.

III. DEDUCING $a_\mu^{(2)\text{had}}$

In order to infer the value of $a_\mu^{(2)\text{had}}$ from our data, we must carry out the integral (2.8) which we split into high- and low-momentum regions at some momentum cut Q_C^2,

$$a_\mu^{(2)\text{had}} = 4\alpha^2 \bigg[\int_0^{Q_C^2} dQ^2 f(Q^2) \times \hat{\Pi}(Q^2) $$
$$+ \int_{Q_C^2}^\infty dQ^2 f(Q^2) \times \hat{\Pi}(Q^2) \bigg]. \quad (3.1)$$

A continuous description of $\Pi(Q^2)$ at low momenta is obtained by performing a fit to our lattice data, which allows us to perform the low Q^2 integral. The value of $\Pi(0)$ from this fit combined with a high-momentum description of $\Pi(Q^2)$ from perturbation theory allows us to perform the high-momentum integral. As we shall see, the integral is strongly dominated by the low-momentum contribution.

A. Fitting the low Q^2 region

We have attempted to fit a continuous form to our lattice data for the vacuum polarization using a number of different fit forms. The effect that the choice of fit function can have on the result for $a_\mu^{(2)\text{had}}$ has been highlighted in previous studies [13], and this behoves us to ensure that the systematics with regard to this choice are under control.

The suitability of a given fit-form should be judged on two main criteria:

(i) Firstly, the chosen expression must describe the data closely, and must do so regardless of the range of data included in the fit. As such, we require the reduced χ^2 of the fit to be consistently low as a function of Q_C^2 which defines the range of data in the fit.

(ii) Secondly, in order to deduce that the fit-form results in an integral over momentum which is relatively stable, we desire that the result for $a_\mu^{(2)\text{had}}$ is again relatively stable as a function of Q_C^2.

Reference [13] also illustrated the use of a fit form originating in the expression for the vacuum polarization calculated in chiral perturbation theory. The dominant component of this expression is due to the vector meson contribution, which at tree level is

$$\Pi_V^{\text{tree}}(Q^2) = \frac{2}{3} \frac{f_V^2}{Q^2 + m_V^2} \quad (3.2)$$

where the vector decay constant f_V is defined

$$\langle \Omega | J_\mu | V, p, \epsilon \rangle = m_V f_V \epsilon_\mu(p). \quad (3.3)$$

Motivated by this expression, the fit-form we use is closely related, differing only in the inclusion of the contribution of an additional vector resonance,

$$\Pi(Q^2) = A - \frac{F_1^2}{Q^2 + m_1^2} - \frac{F_2^2}{Q^2 + m_2^2}. \quad (3.4)$$

The one-loop contribution from the pseudoscalar sector, shown in [13] to have small momentum dependence, will not strongly affect our results and so, in our effort to make a continuous description of the lattice data, it will be omitted from our fit ansatz.

We fit the lattice vacuum-polarization data in two ways:

(i) Firstly, using A, $F_{1,2}$, and $m_{1,2}$ as free parameters.

(ii) Also, fixing the parameter m_1 to the mass of the vector meson m_V as measured in [19]. This we do by constraining m_1 to lie in the one-sigma band defined by the estimate of m_V and its variance. This method was found to maintain the stability of the fit routine, while incorporating the extra information provided by m_V. In this fit, A, $F_{1,2}$, and m_2 remain as true free parameters.

The behaviors of such fits are shown in Fig. 3. Clearly, such a form is a very good representation of the data, over practically the whole range of Q_C^2. In addition, the results for $a_\mu^{(2)\text{had}}$ using such fits are very stable as the fit range is varied, allowing far greater confidence in the reliability of the result. In particular, we conclude that using a fit form (3.4) with the mass of the first pole fixed to the ground-state vector meson mass to be the optimal method of describing the lattice data for the hadronic vacuum polarization.

In Fig. 4, we see the value of the fit parameter m_1 from (3.4) as determined from fits to the lattice vacuum polarization. The value of m_V obtained in [19] is shown in green,
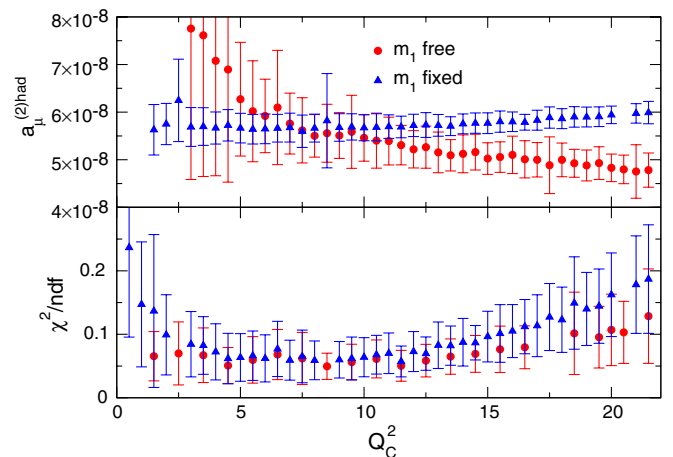

FIG. 3 (color online). Properties of fits to the lattice vacuum polarization using the ansatz (3.4) on the $\beta = 2.25$ lattice at $am_u = 0.004$. Only points for which the fitting procedure was reasonably stable are shown.
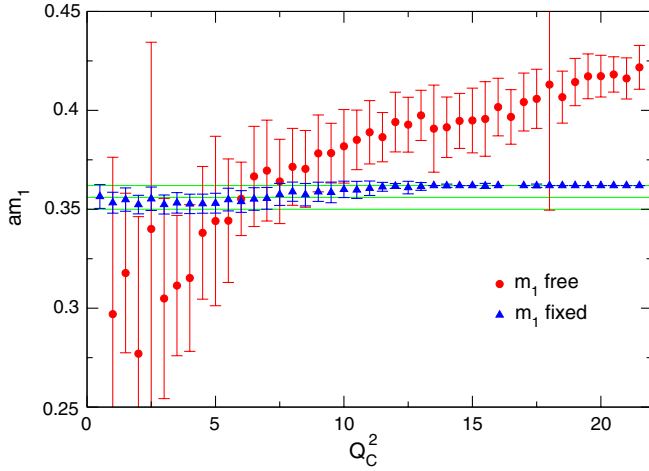
FIG. 4 (color online). Value of the fit parameter am_1 in fits using the ansatz (3.4) on the $\beta = 2.25$ lattice at $am_u = 0.004$. The vector mass am_V as determined on this lattice is shown in green. Note in the fit where m_1 was fixed, it was only constrained to lie within the green band. It is clear that for a high Q_C^2, m_1 will emerge at the upper limit of the band, indicating some tension between the fit-form and the data, but as can be seen in Fig. 3, this has very little impact on the goodness of the fit.

and this defines the band in which m_1 was constrained to reside in the fixed version of this fit. We have not attempted to model $O(4)$ breaking effects present in our data. Though such effects do appear to be present to a moderate degree on certain ensembles, they do not prevent the extraction of a reasonable signal from our data at this point. These effects could also be alleviated by the use of twisted boundary conditions [24].

B. Evaluation of (3.1)

Illustrations of the integrand can be seen in Fig. 5. Because the integrand is dominated by contributions in the low-momentum region, we change our integration measure to better sample the region of interest. To do this, we make the change of variables
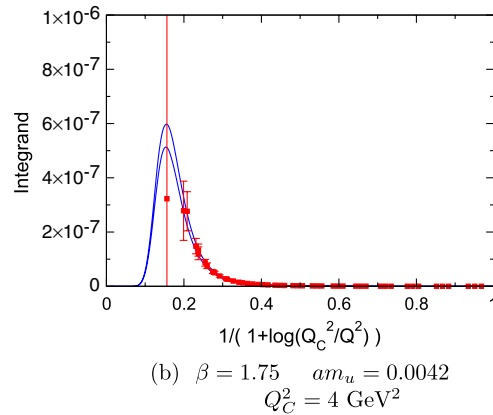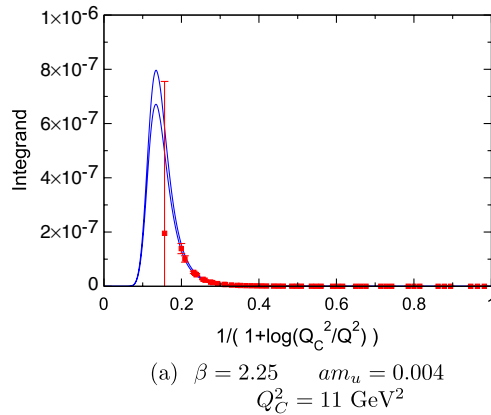
$$t = \frac{1}{1 + \log\frac{Q_C^2}{Q^2}} \tag{3.5}$$

and so the integral over the low-momentum region becomes

$$\int_0^{Q_C^2} dQ^2 f(Q^2) \times \hat{\Pi}(Q^2) \rightarrow \int_0^1 dt f(Q^2) \times \hat{\Pi}(Q^2) \times \frac{Q^2}{t^2}. \tag{3.6}$$

Overlaid on the depiction of the integrand in Fig. 5 is the appropriately subtracted and rescaled vacuum polarization data. We see from this that, while a large portion of the constraint on the fit is consistently derived from data at higher momentum, the fit is always consistent with the data at low momentum, the region where the integral receives the dominant contribution.

In particular, in Fig. 5(b) we see that on the larger lattices at $\beta = 1.75$ using the Iwasaki + DSDR action, the data point at the lowest momentum sits exactly where the integrand reaches a maximum, and there are numerous data points in the dominant region, constraining the fit. Clearly, using lattices of such size will help in obtaining a precise result for this quantity, and this must be combined with the use of twisted boundary conditions [14] in order to access data at lower values of the lattice momentum.

IV. RESULTS

We extract our final results from the fit using (3.4) with the first mass fixed to that of the vector meson as measured on each ensemble. Observing the behavior of the reduced χ^2 as the fit range is varied, we choose a suitable value for Q_C^2 for each ensemble which provides the most reliable result. We attempt to choose a cut which provides a low reduced χ^2 preferably where the parameter m_1 agrees without tension with m_V. This produces the results shown in Table III, where we also quote the reduced χ^2 of the fit, and the resulting values of the remaining associated free parameters.

(a) $\beta = 2.25$ $am_u = 0.004$ $Q_C^2 = 11$ GeV^2

(b) $\beta = 1.75$ $am_u = 0.0042$ $Q_C^2 = 4$ GeV^2

FIG. 5 (color online). Examples of the integrand in the rescaled integral (3.6).

TABLE III. Results for the hadronic contribution to the muon anomalous magnetic moment.

β	am_u	Q_C^2 GeV2	$\frac{\chi^2}{\text{ndf}}$	$a_\mu^{(h)} \times 10^{10}$	aF_1	am_2	aF_2
2.13	0.02	4	0.38(17)	345(16)	0.114(4)	1.48(19)	0.31(5)
2.13	0.01	3.5	0.07(6)	430(22)	0.110(4)	1.50(23)	0.32(7)
2.13	0.005	3.5	0.14(5)	436(50)	0.097(14)	1.16(18)	0.24(3)
2.25	0.008	6	0.18(11)	452(23)	0.079(2)	1.14(4)	0.26(1)
2.25	0.006	6	0.10(6)	484(33)	0.075(3)	1.07(7)	0.24(2)
2.25	0.004	9	0.06(3)	568(29)	0.079(2)	1.23(3)	0.28(6)
1.75	0.0042	2.5	0.16(9)	536(36)	0.108(20)	1.27(20)	0.26(3)
1.75	0.001	2.5	0.27(13)	646(55)	1.06(11)	1.58(61)	0.37(27)

These results are also shown as a function of m_π^2 in Fig. 6, where we compare them to previous $2 + 1$ flavor results from [13]. Also shown is an extrapolation to the physical point, using a quadratic chiral ansatz. This produces a final result for the leading-order hadronic vacuum polarization contribution the anomalous magnetic moment of the muon

$$a_\mu^{(2)\text{had}} = 641(33) \times 10^{-10}. \qquad (4.1)$$

In [15], the integral (2.8) was performed in a slightly different manner. Here, the kernel function in the integrand was altered by replacing the momentum argument Q^2 of $f(Q^2)$ according to $Q^2 \rightarrow Q^2 \times (\frac{H_{\text{phys}}}{H})^2$ for some sensible choice of a hadronic observable H, where H_{phys} denotes the value of the physical value of the chosen observable, and H denotes the value of the observable measured on the lattice in question. The result of this integral is a new quantity $a_{\bar\mu}^{(2)\text{had}}$ which has the same physical limit as $a_\mu^{(2)\text{had}}$. The goal of this modification is to moderate the chiral variation of the integral's result by cancelling the effects of changing hadronic physics as the chiral limit is approached. It was found that setting $H = m_V$ produced a quantity with the correct physical limit with much more moderate chiral variation, allowing for a more powerful chiral interpolation.

We have investigated the use of this method with our data. We show the results of such a calculation in Fig. 7(a), along with an accompanying chiral extrapolation. The chiral variation in this redefined quantity is such that it allows for a linear extrapolation in quark mass. For the lightest point in our simulation, we include the unmodified result outlined in Table III since for this ensemble the
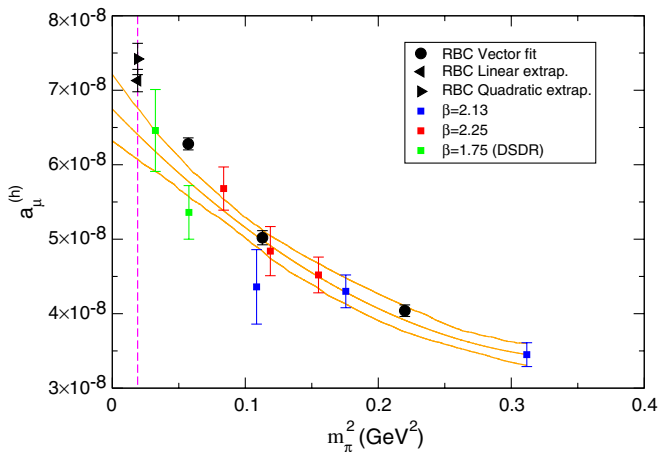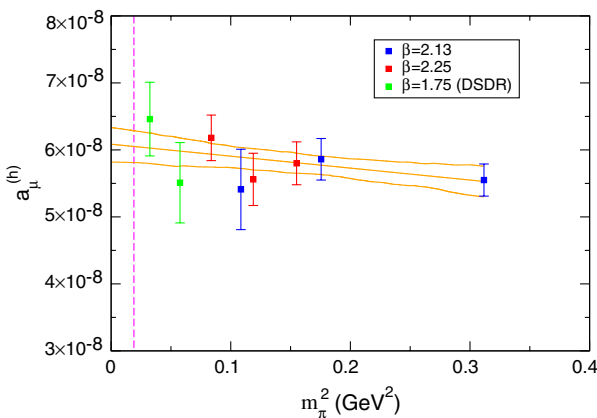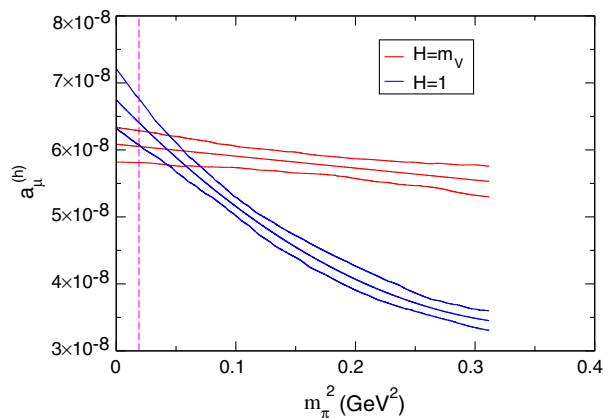

FIG. 6 (color online). Integrated result for $a_\mu^{(2)\text{had}}$ as a function of the pseudoscalar mass squared.

(a) Results using modified prescription $H = m_V$.

(b) Comparison of results from both methods.

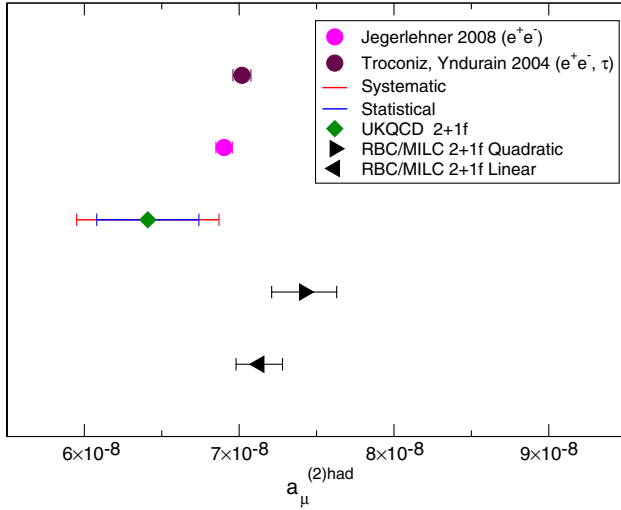FIG. 7 (color online). Analysis of results for modified prescription using $H = m_V$.

FIG. 8 (color online).   Comparison of recent results for $a_\mu^{(h)}$.

measured vector mass m_V is consistent with the physical value. This method does indeed moderate the chiral behavior of the result, however it has little effect on our data at light quark masses, primarily because the lattice vector meson masses are very near that of the physical ρ meson, and, as of now, are not determined to any great precision on these lattices. As such, this technique does not improve our chiral fit at this time, producing a compatible result with a similar uncertainty:

$$a_\mu^{(2)\text{had}} = 605(24) \times 10^{-10}. \tag{4.2}$$

In Fig. 7(b), we compare both chiral extrapolations, with $H = 1$ denoting the standard method, and $H = m_V$ indicating the modified prescription of [15] using the vector mass m_V.

In Fig. 8, our result (4.1) is compared to recent $2 + 1$ flavor lattice results [13] along with a recent result arising from a dispersion integral over experimental data from e^+e^- scattering data. We note that our result appears to be slightly lower than expected, however this could be

TABLE IV.   Comparison of the vector decay constant as measured on our lattices, to the amplitude of the lowest resonance contribution emerging from our fit to the lattice vacuum polarization.

β	am_u	f_V MeV	$\sqrt{\frac{3}{2}}F_1$ MeV	$\sqrt{\frac{3}{2}}\frac{F_1}{C}$ MeV
2.13	0.02		242(10)	179(7)
2.13	0.01		234(8)	166(6)
2.13	0.005		205(30)	144(20)
2.25	0.008	178(13)	221(6)	155(5)
2.25	0.006	174(11)	211(10)	147(7)
2.25	0.004	160(26)	222(5)	155(4)
1.75	0.0042	140(9)	192(27)	129(19)
1.75	0.001	144(20)	179(18)	127(12)

explained by our omission of the disconnected contribution.

In Table IV, we attempt a comparison of the value of F_1 [defined in (3.4)] resulting from our fit, to the vector decay constant as measured on each lattice, according to the relation expressed in (3.2). Note, we do not have a result for f_V on the 64×24^3 lattices at this time, although the ratio of the vector coupling to the vector and tensor currents was studied in [25]. We also make the comparison suggested by the one-loop correction to (3.2) as computed in [13] whereby the relation $F_1^2 \sim \frac{2}{3}f_V^2$ is replaced by $F_1^2 \sim \frac{2}{3}f_V^2 \times C^2$ where

$$C^2 = 1 - \frac{6}{(4\pi f_\pi)^2}\left[m_\pi^2 \log\left(\frac{m_\pi^2}{\mu^2}\right) + m_K^2 \log\left(\frac{m_K^2}{\mu^2}\right)\right] \tag{4.3}$$

with m_π and m_K the pion and kaon meson masses, f_π the pion decay constant, and μ the chiral scale, taken as 1 GeV. In this comparison, we are neglecting the one-loop contribution from the pseudoscalar sector, and so, while neither of these comparisons emerges particularly convincingly, this indicates that the vacuum polarization is reflective of the analytic approximation.

V. CONCLUSIONS

We present a fully dynamical calculation of the leading-order hadronic vacuum polarization contribution to the anomalous magnetic moment of the muon, using a $2 + 1$ flavor simulation lattice QCD using domain wall fermions. Although we have an expensive fermion discretization, we improve the accuracy of our result by convolving an accurate determination of the ground-state vector meson mass with our determination of the lattice hadronic vacuum polarization in order to suppress the systematic uncertainty associated with the choice of fit ansatz. Our chiral extrapolation involves lattices at different bare couplings, and thus different lattice spacings, however at this level of precision we do not detect any significant discretization, or finite volume errors in our result. Our final result we take to be

$$a_\mu^{(2)\text{had}} = 641(33)(32) \times 10^{-10} \tag{5.1}$$

where the first error is statistical and the second is an estimate of the systematic error arising from the extrapolation to the chiral limit, taken as 5%, motivated by the variation between the results (4.1) and (4.2). Our largest systematic uncertainty arises from the omission of the disconnected contributions and is of the order of 10% [26]. In order to obtain a more comprehensive and accurate result, we must include the disconnected contributions in our calculation. Furthermore, this being a first effort at deducing this quantity from our lattices, we have plans to improve it in a number of ways. In addition to the enhancement of our statistics, we would like to obtain a higher-momentum resolution through the use of twisted boundary

conditions, and also to explore the use of stochastic sources to further enhance our signal.

ACKNOWLEDGMENTS

[1] Julian S. Schwinger, Phys. Rev. **73**, 416 (1948).
[2] D. Hanneke, S. Fogwell, and G. Gabrielse, Phys. Rev. Lett. **100**, 120801 (2008).
[3] S. Laporta and E. Remiddi, Nucl. Phys. B, Proc. Suppl. **181–182**, 10 (2008).
[4] G. W. Bennett *et al.*, Phys. Rev. D **73**, 072003 (2006).
[5] Fred Jegerlehner and Andreas Nyffeler, Phys. Rep. **477**, 1 (2009).
[6] Masashi Hayakawa, Thomas Blum, Taku Izubuchi, and Norikazu Yamada, Proc. Sci., LAT2005 (2006) 353.
[7] T. Blum and S. Chowdhury, Nucl. Phys. B, Proc. Suppl. **189**, 251 (2009).
[8] F. Jegerlehner, Nucl. Phys. B, Proc. Suppl. **181–182**, 26 (2008).
[9] Eduardo de Rafael, Phys. Lett. B **322**, 239 (1994).
[10] T. Blum, Phys. Rev. Lett. **91**, 052001 (2003).
[11] M. Göckeler and others, Nucl. Phys. **B688**, 135 (2004).
[12] T. Blum, Nucl. Phys. B, Proc. Suppl. **129–130**, 904 (2004).
[13] C. Aubin and T. Blum, Phys. Rev. D **75**, 114502 (2007).
[14] Michele Della Morte, Benjamin Jager, Andreas Jüttner, and Hartmut Wittig, J. High Energy Phys. 03 (2012) 055.
[15] Xu Feng, Karl Jansen, Marcus Petschlies, and Dru B. Renner, Phys. Rev. Lett. **107**, 081802 (2011).
[16] Shigemi Ohta for the RBC Collaboration and the UKQCD Collaboration, arXiv:1111.5269.
[17] RBC Collaboration and UKQCD Collaboration, Continuum Limit Physics from $2 + 1$ Flavor Domain Wall QCD II.
[18] C. Allton *et al.*, Phys. Rev. D **78**, 114509 (2008).
[19] Y. Aoki *et al.*, Phys. Rev. D **83**, 074508 (2011).
[20] Vadim Furman and Yigal Shamir, Nucl. Phys. **B439**, 54 (1995).
[21] Peter A. Boyle, Luigi Del Debbio, Jan Wennekers, and James M. Zanotti, Phys. Rev. D **81**, 014504 (2010).
[22] Michele Della Morte and Andreas Jüttner, J. High Energy Phys. 11 (2010) 154.
[23] K. G. Chetyrkin, Johann H. Kuhn, and M. Steinhauser, Nucl. Phys. **B482**, 213 (1996).
[24] R. Arthur and P. A. Boyle, Phys. Rev. D **83**, 114511 (2011).
[25] D. Antonio, P. A. Boyle M. A. Donnellan, J. Flynn, A. Juttner, C. Maynard, B. Pendleton, C. T. Sachrajda, and R.Tweedie, Proc. Sci., LAT2007 (2007) 369.
[26] Andreas Jüttner and Michele Della Morte, Proc. Sci., LAT2009 (2009) 143.
[27] P. Boyle *et al.*, Nucl. Phys. B, Proc. Suppl. **140**, 169 (2005).
[28] P. A. Boyle, C. Jung, and T. Wettig, in *The QCDOC Supercomputer: Hardware, Software, and Performance*, econf C0303241, THIT003, THIT002, THIT001 (2003).